HHS Public Access

Author manuscript

Cell Rep. Author manuscript; available in PMC 2020 November 19.

Published in final edited form as:

Cell Rep. 2020 October 20; 33(3): 108272. doi:10.1016/j.celrep.2020.108272.

Motivation and Engagement during Visually Guided Behavior

Alexander V. Ortiz[1], **David Aziz**[2], **Shaul Hestrin**[1,3,*]

[1]Department of Comparative Medicine, Stanford School of Medicine, Stanford, CA 94305, USA

[2]College of Optical Sciences, University of Arizona, Tucson, AZ 85721, USA

[3]Lead Contact

SUMMARY

Animal behavior is motivated by internal drives, such as thirst and hunger, generated in hypothalamic neurons that project widely to many brain areas. We find that water-restricted mice maintain stable, high-level contrast sensitivity and brief reaction time while performing a visual task, but then abruptly stop and become disengaged. Mice consume a significant amount of water when freely provided in their home cage immediately after the task, indicating that disengagement does not reflect cessation of thirst. Neuronal responses of V1 neurons are reduced in the disengaged state, but pupil diameter does not decrease, suggesting that animals' reduced level of arousal does not drive the transition to disengagement. Our findings indicate that satiation level alone does not have an instructive role in visually guided behavior and suggest that animals' behavior is governed by cost-benefit analysis that can override thirst signals.

In Brief

Ortiz et al. study performance of mice in a visual task during engagement and disengagement. Mice disengage from the task without reaching satiation. Pupil diameter indicates that reduced alertness is not associated with disengagement. We suggest that areas downstream of visual cortex perform cost-benefit analysis governing response to thirst signals.

Graphical Abstract

*Correspondence: shestrin@stanford.edu.

AUTHOR CONTRIBUTIONS

Conceptualization, S.H., A.V.O.; Methodology, S.H., A.V.O., D.A.; Investigation, S.H., A.V.O.; Software and Formal Analysis, S.H., A.V.O.; Resources, S.H.; Writing, S.H., A.V.O.; Funding, S.H.

DECLARATION OF INTERESTS

The authors declare no competing interests.

SUPPLEMENTAL INFORMATION

Supplemental Information can be found online at https://doi.org/10.1016/j.celrep.2020.108272.

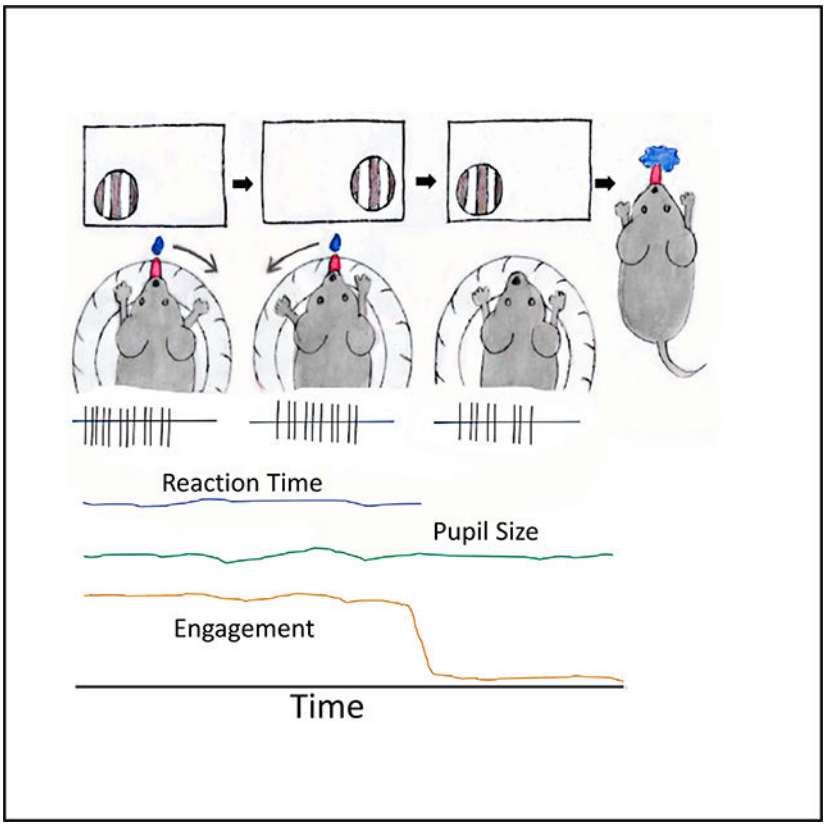

INTRODUCTION

Study of sensory perception often requires restricted water or food consumption to create motivational drive. Drive reduction theory of motivation posits that physiological needs function as negative reinforcers (Berridge, 2004), and that by consuming water or food, animals reduce unpleasant or aversive stimuli. Thus, this theory implies that within a behavioral session, animal ingestion activity would diminish physiological needs and therefore weaken motivational drive (Allen et al., 2017; Betley et al., 2015; Leib et al., 2017). Given that the physiological effect of water ingestion is incremental, it is expected that during behavioral sessions, animals' motivation will exhibit gradual diminishment. In support of this view, recent recordings in hypothalamic nuclei have shown that activity of thirst-sensitive neurons is reduced gradually over a course of 10 min and is correlated with the volume of water consumption (Allen et al., 2017). If animals' behavior is directly controlled by their level of satiation, their perceptual performance may change gradually, reflecting their level of thirst and water consumption during behavioral sessions. For example, within a behavioral session, an animal's reduced drive may result in increased reaction time and reduced response rate to weak stimuli. To test these predictions, we trained mice in a two-alternative forced-choice (2AFC) visual task (Burgess et al., 2017) and tested their contrast sensitivity, reaction time, neuronal response, and pupil parameters during behavioral sessions. Mice performed several hundred trials and then abruptly stopped and became disengaged. However, under these conditions, mice were not satiated and readily

consumed a significant amount of water when offered *ad libitum* in their home cage. We showed that when mice were engaged in the task, their perceptual performance was stable, and that the transition to disengagement was associated with reduction of neuronal response.

RESULTS

Animals were head fixed and their paws rested on a wheel, which they learned to rotate (Burgess et al., 2017). The movement of the wheel was converted to the angle of the stimulus in the mouse's field of view. Stationary, sinusoidal gratings of variable contrast were presented in a square aperture on either the left or right of the screen. The mouse indicated its choice by moving the visual stimulus into the center of the screen by rotating the wheel in the necessary direction (Figure 1A). A 1-s quiescent period was enforced during which the mouse had to keep the wheel still in order to initiate the appearance of a visual stimulus. If the mouse remained quiescent for a sufficient time, an auditory cue and visual stimulus were presented, and a closed-loop session began where the wheel's position and the position of the visual stimulus were coupled and the mouse was able to move the stimulus freely across the screen by rotating the wheel (Figure 1A). Mice had to move the stimulus to the center in order to receive a water reward. Rotation of the wheel in the incorrect direction was classified as an error and was followed by the immediate disappearance of the visual stimulus and a repetition of the trial in which the visual stimulus was presented on the same side (see STAR Methods; Figure 1A).

Mouse performance was tested by presenting stimuli of various contrasts (1.2%, 4%, 8%, 16%, 32%, and 64%). We generated psychometric curves for contrast sensitivity and estimated their contrast threshold and bias by calculating the best fit using Equation 1 (see STAR Methods; Figure 1B). Contrast threshold, bias, and lapse rates were stable across sessions (mean: 10.11% ± 3.31%, 0.16% ± 3.21%, and 6.43% ± 2.22% respectively; n = 5 mice over 5 sessions) (Figure 1C). Optogenetic silencing at the onset of the visual stimulus delayed the behavioral response, demonstrating that intact V1 is necessary for this behavioral task (STAR Methods; Figure S1A).

In 2AFC, the rate of miss trials (referred to as miss rate) indicates the level of task engagement. We found that expert mice exhibited negligible miss rate while performing the task (Figure 1D, bottom panel). However, after consuming about 0.6 mL of water they became disinterested in the task, stopped moving the wheel, and became disengaged. This behavioral transition was marked by a sharp rise in the miss rate (Figure 1D). We analyzed the running miss rate (in blocks of 10 trials) of mice over the course of the sessions (5 mice; 30 sessions). We found that there was typically a clearly discernible point in time where mice stopped performing the task and the miss rate increased from less than 3% to over 60% and remained very high for the later portion of the session (Figure 1D; Figure S1C). We continued running the behavioral task for approximately 50 trials after they became disinterested and stopped performing.

To determine whether the transition from engaged to disengaged was mediated by satiation, we provided mice additional water (0.5 mL) in a small dish immediately after behavioral testing. Mice drank 0.29 ± 0.01 mL of the provided water after already having consumed

0.55 ± 0.02 mL (n = 76 sessions, n = 7 mice) during the session, indicating that they were not satiated when switching from engaged to disengaged behavior.

Does performance change as mice ingest water and approach the disengagement period? We generated psychometric curves for the first and second halves of the engagement period (Figures 1E1 and 1E2; Figure S1C). Bias and lapse rate did not change significantly over the course of a behavioral session, and contrast threshold showed a small but significant decrease over the course of a session (5 mice, 23 sessions; Figure S1C). One possible explanation for this observation is that it may take several trials for mice to "warm up" before they reach peak performance.

Previous studies have found that pupil diameter correlates with cognitive effort and performance (Erisken et al., 2014; Kahneman and Beatty, 1966; McGinley et al., 2015a; Reimer et al., 2014, 2016; Vinck et al., 2015). We asked whether pupil diameter during the 1 s preceding the appearance of the stimulus could predict performance. We divided the trials into two groups based on whether the pupil diameter was larger or smaller compared with the average pupil diameter (Figures 1F1 and 1F2). We found that the bias, contrast threshold, and lapse rate were not different when comparing small and large pupil diameters (Figure S1D). The average pupil diameter was about 10% larger during the disengagement period, suggesting that mice did not reduce their level of arousal during the disengagement period ($p = 0.0013$, Wilcoxon signed rank; n = 27 sessions). Together these data indicate that mice maintained stable, high-level task engagement and performance before switching abruptly to a disengaged state without reaching satiation, and that disengagement was not associated with reduced level of arousal.

During the disengagement period, mice exhibited brief intervals during which they responded to the presented stimuli (Figures 1D and 3B). We found that during the disengagement period, mice preferentially responded to high-contrast (16%, 32%, and 64%) stimuli over low-contrast (1.2%, 4%, and 8%) stimuli (response rates: 0.57 and 0.30, respectively; $p = 1.18 \times 10^{-5}$, n = 30 sessions, 5 mice). However, the hit rate in response to low-contrast stimuli did not change across the engaged and disengaged states (0.65 ± 0.028 and 0.65 ± 0.046, respectively; $p = 0.987$). These data suggest that when mice responded to stimuli, their contrast sensitivity was comparable across the engagement-disengagement periods.

To study the impact of engagement on single-unit response, we next trained a second cohort on an open-loop, high-contrast (64%) stimulus behavioral task (Figure 2A). In this task, mice were required to indicate their choice by rotating the wheel, but the stimulus did not move and remained within the cell's receptive field. Mice trained on the open-loop task showed a sharp transition from engagement to disengagement, which was comparable with their behavior in the closed-loop 2AFC task (Figure 2B). During the engagement period, mice had a high hit rate (95.5% ± 0.53%) and maintained a stable response latency (0.38 ± 0.03 s; n = 7 mice, n = 51 sessions; Figure S2B). We found that pupil diameter did not significantly change when comparing the engaged and the disengaged periods ($p = 0.67$, Wilcoxon signed rank test; n = 36 sessions). The transition to disengagement was associated with a significant increase in eye position variance but with a largely overlapping range

(Figure 2C, middle panels; Figures S2C and S2D). Together, these data show that animals can maintain a prolonged period of task engagement during which their eye position and pupil diameter generally remain unchanged, possibly optimizing their performance (McGinley et al., 2015a). After switching to disengagement, pupil parameters (diameter and position) remain similar to those during engagement but exhibit larger variation (Figures S2C and S2D).

Previous studies have shown that mouse V1 neurons increase their response to visual stimuli by 2-fold or more during locomotion (Bennett et al., 2013; Niell and Stryker, 2010; Polack et al., 2013). This increased visual response may be related to a change in cognitive state and/or locomotion-related circuits affecting V1 cells (McGinley et al., 2015b; Vinck et al., 2015). Under our experimental conditions, mice changed their behavioral state but remained stationary. Therefore, we asked whether the self-initiated transition from engagement to disengagement affects neuronal activity in stationary animals. We recorded single-cell spiking in V1 and compared their responses with visual stimuli during the engagement and disengagement periods. We first used local field potential (LFP) recordings to determine the receptive field of cells located within a small craniotomy. Next, using loose-seal recordings, we identified individual neurons that responded to visual stimuli placed at the LFP-located receptive field and determined their direction preference (see STAR Methods). We then initiated an open-loop behavioral session with a fixed, high-contrast (64%) drifting gratings stimulus at the cell's preferred direction (Figure 3A). In this task, mice reported the location of the stimulus by rotating the wheel, but the stimulus location was fixed (Figure 3A). During the engagement period, the mouse had near 100% hit rate (Figure 3B, left panel). Stimulus-triggered peri-stimulus time histograms (PSTHs) demonstrated a fast rise in spike rate preceding the rotation onset by several hundred milliseconds (Figure 3B). The spontaneous spike rates (measured 1 s prior to stimulus presentation) were comparable across engagement and disengagement periods (6.21 ± 0.34 and 5.59 ± 0.29, respectively; n = 16 cells; p = 0.72). During the engagement period, the average neuronal response in all trials (hit and miss) was significantly stronger compared with neuronal responses during the disengagement period (Figures 3B and 3C, bar plots). During the engagement period, spike count in the interval between stimulus presentation and rotation onset was significantly larger than during the disengagement period (5.11 ± 0.92 versus 3.84 ± 0.70; p = 0.009; n = 16 cells; all trials). In addition, the stimulus-induced spike count for the entire stimulus duration was significantly larger during the engagement period than during the disengagement period (30.95 ± 3.99 versus 22.19 ± 3.39; p = 0.033; n = 16 cells; all trials; Figures 3B and 3C; Figure S3C). Furthermore, we found that when aligned to the transition point between the engagement period and the disengagement period, the average spike count for contralateral stimulation showed a sharp decrease at the point of disengagement, consistent with the abrupt change in behavior indicated by the onset of the disengagement state (Figure S3A).

During the engagement period, the rate of trials classified as miss trials was less than 5%, whereas during the disengagement period the rate of miss trials was about 60% (Figure 2B). Therefore, the reduced spike count for trials during the disengagement period could, in part, reflect reduced motor activity (Dipoppa et al., 2018; Musall et al., 2019; Niell and Stryker, 2010; Salkoff et al., 2020) during miss trials (which represent the majority of trials). We

found that during disengagement, the average spike count for hit trials was larger than the average spike count for miss trials (25.21 ± 4.78 and 19.08 ± 3.42, respectively; n = 16 cells; p = 0.025; Figure S3B, right panel). In addition, we found that the spike count for hit trials during the engagement period was on average larger than the spike count for hit trials during the disengagement period (30.13 ± 4.18 and 25.21 ± 4.78, respectively; n = 16 cells; p = 0.07; Figure 3SB, left panel). These data suggest that there is a relatively modest reduction of spike count across engagement and disengagement states or in association with wheel rotation.

DISCUSSION

Animals performed at a high level in a 2AFC task for a prolonged period of time but then stopped responding to reward-delivering stimuli and disengaged from the task. This change in behavioral state of stationary animals was abrupt, as indicated by the sharp increase of their miss rate. It is often assumed that when animals stop responding to reward-delivering stimuli they have reached satiation. However, mice readily drank additional water in their home cage. Therefore, the disengaged state did not reflect complete satiation. Furthermore, we found that disengagement was not associated with reduction of the average pupil diameter, suggesting that reduced level of arousal did not have a causal role in the transition to the disengaged behavioral state. Why did mice disengage from the task without reaching complete satiation? We propose a two-step model. In the first stage, a signal reflecting the level of thirst generated in hypothalamic nuclei (and other areas) broadcasts across multiple brain regions (Allen et al., 2017, 2019; Betley et al., 2015; Leib et al., 2017). In the second stage, the strength of the thirst signal is tested against a threshold set by higher brain areas, including cortical areas. If the thirst signal exceeds the threshold, mice will emit an all-or-none water-seeking behavior that does not reflect the strength of the thirst signal. We further propose that, under our experimental conditions, the threshold reflects the level of cognitive effort required to perform the task. When mice ingest water during our behavioral task, the activity of *lamina terminalis* neurons gradually declines (Allen et al., 2017). When that signal falls below the threshold, mice will abruptly stop responding to the task. However, when water is subsequently made freely available, thus reducing the effort required to obtain it, mice will resume drinking. Moreover, if after mice stop drinking the thirst signal is increased by external stimulation, it will exceed the threshold, resulting in resumed drinking as was observed by Allen et al. (2017) (Leib et al., 2017).

Does the thirst signal affect behavioral performance? We showed that contrast threshold, bias, lapse rate, and reaction time were stable during the engagement period when mice were consuming water over a period of 30–60 min. Stable, high-level behavioral performance during prolonged behavioral sessions has been previously observed in non-human primates (e.g., Britten et al., 1996). Therefore, we suggest that the level of thirst contributes to motivation but does not impact the perceptual performance in mice (and possibly other species) as implied by the two-stage model we propose.

Visual responses of V1 neurons during the engagement period were stronger than their responses during the disengagement period. Change of visual response strength of V1 neurons of mice was also observed in comparing neuronal activity of V1 neurons during

locomotion and stationary state (Bennett et al., 2013; McGinley et al., 2015a, 2015b; Niell and Stryker, 2010; Polack et al., 2013). It was previously shown that motor activity is associated with brain-wide excitation and can therefore generate the increased visual response of V1 neurons (Dipoppa et al., 2018; Musall et al., 2019). Recently, it was found that activation of V1 neurons in stationary mice changes in response to removal of reward availability (Steinmetz et al., 2019; see also Speed et al., 2020). Can the decreased visual response of V1 neurons underlie the transition to disengagement? In principle, suppression of the visual response would propagate a weaker signal downstream that is not sufficiently strong to produce a behavioral response. It is, however, unlikely given the relatively modest response reduction to high-contrast stimuli during disengagement. These reduced responses would be comparable to responses to lower contrast stimuli, suggesting a shift in the contrast sensitivity during disengagement. In contrast, we found that performance parameters were stable throughout the engagement period and observed a substantial cessation of response during the disengagement period. Together these data suggest that reduced response of V1 neurons does not have a causal role in the transition to disengagement. Thus, we propose that downstream areas veto visual inputs when the animals are disengaged.

In summary, our data suggest that thirst-related signals originating from subcortical nuclei can be overruled by other brain areas, possibly including the cortex (Leib et al., 2016), that can govern drinking behavior. These findings suggest that animal behavior is flexible and the result of a complex interplay between internal drives and the cognitive-motor costs associated with drinking.

STAR★METHODS

RESOURCE AVAILABILITY

Lead Contact—Further information and requests for resources and reagents should be directed to and fulfilled by the Lead Contact, Shaul Hestrin (shestrin@stanford.edu)

Materials Availability—This study did not generate new unique reagents.

Data and Code Availability—The datasets and code supporting the current study have not been deposited in a public repository but are available from the corresponding author on request.

EXPERIMENTAL MODEL AND SUBJECT DETAILS

Mice—All procedures were approved by the Administrative Panel on Laboratory Animal Care at Stanford University. Two or more mice (C57BL/6j; JAX Stock 664; males and females ages 12 – 16 weeks old) were housed in a rat cage that included a running wheel and a small cardboard box that allowed for nest building.

METHOD DETAILS

Headplating—All surgical procedures were carried out aseptically on adult mice (males and females ages 12 – 16 weeks old). Mice were anesthetized using 10 mg/mL of ketamine-HCL (0.01 mL per gram of body weight) and 1.25 – 2% isoflurane, mounted in a stereotaxic

instrument and placed on a heating pad to maintain body temperature at 38°C. Body temperature was monitored with a rectal probe during the operation. Petrolatum ophthalmic ointment was applied directly to eyes to prevent damage and excessive dryness. The mouse's scalp was cleaned with ethanol followed by a coat of betadine scrub. This procedure was repeated 3 times. Next, 0.2 mL of 1 mg/ml Lidocaine was injected directly into the mouse's scalp and a circular piece of scalp approximately 12 mm in diameter was removed. The underlying skull was cleaned with a metal scraping instrument and hydrogen peroxide was applied to the bone with a cotton applicator. A custom-made head-fixation titanium ring with a 10 mm internal diameter was positioned on the exposed skull and cemented in place using Metabond dental acrylic (S399 Clear-3gms L-powder Parkell A00293revA306).

Craniotomy—After head-plating, Metabond dental acrylic over V1 (±2500 μm lateral and +100 μm anterior to lambda) was thinned to expose the underlying skull. Next, the skull was carefully thinned until transparent. Saline was applied to the drilling site to cool it down and flush out fragments of bone and cement. Thin, sharp forceps were used to slice through the thinned, softened skull and excise a disc of bone to make a craniotomy ~250 μm in diameter. After removal of the bone, the craniotomy was flushed with saline, lightly dried with a cotton applicator, and covered with Quick-cast gel. Once the Quick-cast was set, the animal was removed from the surgical set-up and allowed to recover in a clean cage for at least 2 hours before behavioral testing. The quick-cast plug was removed prior to testing and was replaced at the end of the behavioral experiments.

Optogenetic silencing—The transparent skull technique was conducted on mice that had previously been head-plated. After head-plating, Metabond dental acrylic was thinned, smoothed, and cleaned to increase the transparency of the skull for optogenetic silencing (Guo et al., 2014; Hira et al., 2009). Optogenetic silencing was carried out by utilizing blue light (470 nm, 5–10 mW) epi-illumination to inhibit cortical activity in V1 of both hemispheres in VGAT-ChR2-EYFP animals during task performance. Optogenetic silencing was delivered randomly on 30% of trials.

Rig Set-up and Wiring—We constructed a behavioral rig to train animals on the 2AFC task. The rig was composed of 4 Dell PC computers, 2 Arduino-2560 microprocessors, 1 solenoid driver, 1 solenoid valve, 1 infrared lickport, 1 Piezoelectric spark speaker, 1 YUMO 6mm 1024 P/R rotary encoder, 1 PCO.edge 4.2 imaging camera (PCO), 1 Guppy firewire camera, and 1 MAKO USB camera (Allied Vision). One of the computers was responsible for running the virtual reality program Unity software (Unity Technologies) and received inputs from one of the Arduinos which continuously sampled the rotary encoder and solenoid driver to collect wheel rotation and lick data, respectively. The Unity program read the Arduino's inputs via a serial line and updated the position of stimuli on the screen based on the Arduino's signals. A second Arduino received inputs from Unity and activated the solenoid driver (to trigger water rewards) and in addition, triggered the ITC-18 data acquisition software and cameras. The solenoid driver monitored licks via the lickport and sent lick data to the first Arduino. Additionally, when triggered by the second Arduino, the solenoid driver opened the solenoid valve to release water rewards. The PCO.edge 4.2 camera (PCO Germany) was used to direct pipettes to craniotomies for LFP and single-unit

recordings. The Guppy/Mako cameras (Allied Vision) were utilized to monitor the pupil, licks, whisking, and paw movements of behaving animals. Infrared LEDs were mounted on the cameras and programmed to deliver 20 ms flashes at the beginning of a trial allowing videos and behavioral data to be synced.

Behavioral Training—The general methods that we used to train mice in 2AFC task were similar to those described by Burgess et al. (Burgess et al., 2017). To prepare for behavioral training, mice were water-restricted (0.4–0.6 mL per animal) for 72–96 hours (or until mice were just above 80% of their baseline body weight). We weighed animals daily and their weight was kept above 80% of their baseline body weight. Animals were head-fixed to a stainless steel head-fixation fork via cemented Titanium headplate and placed in a plastic tube (4.5 cm in diameter) that contained the entirety of their body excluding their head and front paws which protruded from the front opening. Their paws rested on a Lego motorcycle wheel which they learned to rotate.

We measured the rotation angle of the wheel with an optical encoder (YUMO 6mm 1024 P/R) which was read using an Arduino microprocessor. The wheel's position was coupled to the position of a visual stimulus (sinusoidal grating 0.05 cycles/degree, 100% Michelson contrast) using Unity Technologies system. The stimuli were displayed on a monitor (Asus; 60 cm X 33 cm; maximum illuminance: 43.5 lux) placed 20 cm in front of the animals (extending 142 degrees X 88 degrees). The movement of the wheel was converted to the angle of the stimulus in the mouse's field of view. Gratings of various contrasts (1.2%, 4%, 8%, 16%, 32%, and 64%) were presented on the right or left of the screen center. The mouse indicated its choice by moving the visual stimulus into the center of the screen by rotating the steering wheel in the necessary direction.

A trial began with a 50% luminance gray screen. A one second quiescent period was enforced during which the mouse had to keep the wheel still in order to initiate the appearance of a visual stimulus. If the mouse remained quiescent for sufficient time, the visual stimulus appeared, a go-tone (5 kHz, 100 ms) was played from a speaker and a closed loop session began where the wheel's position and the position of the visual stimulus were coupled and the mouse was able to move the stimulus freely across the screen by rotating the wheel. Stimuli were randomized to appear either on the right or left and mice had to move the stimulus to the center in order to receive a water reward of 4 μL per correct choice. An error was classified as rotation of the wheel 30 degrees in the incorrect direction and was followed by the immediate disappearance of the visual stimulus and a repetition of the trial in which the visual stimulus was presented on the same side. If a mouse erred more than ten times in a row, the position of the visual stimulus on the next trial was randomized once again. If a mouse did not move the wheel or moved less than 30 degrees in either direction, the trial was classified as a "miss."

Untrained mice rarely moved the wheel on their own, so for the first 3 to 5 days of training, the wheel was manually operated and slowly rotated in the correct direction to help mice develop an association between wheel movement and reward. After mice reached stable performance (~80% hit rate) on stimuli with 100% contrast, lower contrast stimuli (64%, 32%, 16%, 8%, 4%, and 1.2%) were introduced.

Before training mice in the open-loop task, we first trained them in the closed-loop task. When they reached 80% hit rate for high-contrast stimuli (64%) we switched the task to an open-loop task.

LFP recordings & Retinotopic Mapping—A head-fixed mouse was mounted on the behavioral training rig and the quick-cast plug was removed from its craniotomy. The PCO.edge imaging camera was used to direct pipettes (2.53 MΩ, 0.6 PSI) over the craniotomy and lowered until resistance increased, indicating that the pipette was making contact with the dura. The manipulator controlling the pipette was zeroed and the pipette was slowly lowered diagonally until the resistance dropped to its baseline value, signaling the dura had been pierced and the pipette was resting inside the brain. The pressure of the pipette was lowered to 0.2 PSI and the pipette was lowered to a depth of 300 μm while in voltage clamp. White squares (20 degrees in size; 50 ms duration) were continuously presented (1015 repetitions) in a predetermined order at fixed positions on the monitor against a 100% black background. During the stimulus presentation, the local field potential was recorded using standard current clamp techniques and averaged for each stimulus position across all repetitions. The coordinates of the square that had the average LFP with the largest peak was recorded.

Single-unit recordings—The grating stimulus was centered on the coordinates of the square stimulus position that had the average LFP with the largest peak. The mouse was started on a modified version of the behavioral task in which the stimulus was presented for 8 s with drifting gratings that would switch between 8 drift directions every second. Therefore, on each trial, the mouse was presented with gratings that drifted in 8 directions on either the left or right side of the monitor. The pipette was lowered diagonally in voltage clamp until the resistance increased indicating the presence of a nearby cell. The pressure was lowered to zero PSI and the pipette was held near the cell until the stimulus was presented on the contralateral side. The cell's responses to each drift direction were analyzed online. If the cell was not responsive to the stimulus, the pressure was increased to 0.6 PSI and the pipette was lowered diagonally once again until the resistance dropped to the baseline value. Once the resistance returned to baseline, the pressure was decreased to 0.2 PSI and lowered diagonally until a new cell was found. If the cell was responsive to the stimulus, the preferred drift direction was identified and recorded. Next, we started a new behavioral task with a 2 s drifting grating stimulus of the preferred direction. The cell was held and recorded from for the entirety of the behavioral session and the responses were saved using an ITC-18 data acquisition system (Wavemetrics; Igor Pro 6). Cells that were lost in the middle of the session were discarded from further processing and analysis. We confirmed that eye position was similar across behavioral states (Figure S2).

Electrical signals were filtered with a 1st-order high-pass Butterworth filter with cut-off frequency of 150 Hz (Mathworks; MATLAB). For each cell, a maximum spike threshold and minimum spike threshold were empirically determined. Local maxima on the electrode signal were identified and those with values below the maximum spike threshold were eliminated from consideration. For each remaining maximum, a corresponding local minimum (within 15 samples of the local maximum) was identified. If the minimum was

below the minimum threshold, the maximum-minimum pair were determined to correspond to a single spike, otherwise the pair was deemed to be an artifact and eliminated from consideration. The remaining maximum-minimum pairs were deemed single-unit responses (with the maxima corresponding to the signal onset) and utilized for subsequent spike analyses. PSTHs (bin size: 10 ms) were constructed aligned to stimulus onset and included 1 s interval preceding stimulus onset. The PSTHs were smoothed using a Gaussian window of ~30 ms (MATLAB's 'smoothdata' function).

QUANTIFICATION AND STATISTICAL ANALYSIS

Performance Analysis—We computed the percentage of hit trials when stimuli were on the right or left as a function of contrast. Stimuli that appeared on the right and left were represented as positive and negative on the x axis, respectively. Thus, the contrast of stimuli on the left are negative (−100% to 0%) and the contrast of stimuli on the right are positive (0% to 100%). Hit rates for stimuli on the left were subtracted from 100%. Therefore, a perfect hit rate for stimuli on the right would be 100% and a perfect hit rate for stimuli on the left would be 0%. The psychometric curves were fitted with the following function:

$$f(c) = 100 * (L + (1 - 2 * L) * \mathrm{CumNor}(c, \mu, \sigma)) \quad \text{(Equation 1)}$$

where c is the grating's contrast, f(c) is the hit rate, CumNor is cumulative normal distribution, μ is the mean (i.e., bias) and σ is the standard deviation of the underlying normal distribution and L is the lapse rate (Busse et al., 2011). L, μ, σ, were estimated using least-square algorithm (Igor Pro 8 and MATLAB). We defined the standard deviation of the fitted function as the contrast threshold (Busse et al., 2011). We found that the contrast thresholds estimated using maximum likelihood algorithm (MATLAB, fminsearchbnd) were comparable to those estimated with LSE algorithm (Figure 1, n = 5 sessions; p = 0.6). The latency of the response in hit trials was defined as the time interval between stimulus onset and 5-degree rotation.

Pupil Detection and Analysis—We used a Guppy firewire CCD camera (Allied Vision model 031B; 25 mm /F1.4 lens, Edmund Optics) to record videos (50 Hz) of the mouse's eye. We programmed a MATLAB script to identify a mouse's pupil from videos and fit an ellipse to it. We recorded the length of the major axis of the ellipse as well as the x and y position of the center of the ellipse relative to a corneal reflection (produced by an infrared LED directed at the mouse's eye) in pixels for every frame of the video. We then converted the pixels to microns and used the equation E = arcsin((CR - P) / Rp) (where CR is corneal reflection position, P is pupil position, and Rp is radius of pupil: 1.084 mm) to estimate relative horizontal and vertical angles of rotation of the pupil. We estimated the pupil diameter as the length of the major axis of the ellipse. The horizontal and vertical positions relative to the corneal reflection of the center of the pupil were averaged across all frames and deviations from this average on individual frames were used to determine the movement of the mouse's pupil during the course of the session.

Other Analysis—All paired statistical comparisons were performed with the two-tailed Wilcoxon signed-rank test. Non-paired comparisons were performed with two-tailed

Wilcoxon rank-sum test. Averages are reported as mean ± s.e.m. All analysis was performed in MATLAB.

Supplementary Material

Refer to Web version on PubMed Central for supplementary material.

ACKNOWLEDGMENTS

We thank Mateo Carandini and Nick Steinmetz for advice related to the behavioral apparatus and Naomi Zamir for graphical design. This work was supported by NIH grant R01 EY02708701.

REFERENCES

Allen WE, DeNardo LA, Chen MZ, Liu CD, Loh KM, Fenno LE, Ramakrishnan C, Deisseroth K, and Luo L (2017). Thirst-associated preoptic neurons encode an aversive motivational drive. Science 357, 1149–1155. [PubMed: 28912243]

Allen WE, Chen MZ, Pichamoorthy N, Tien RH, Pachitariu M, Luo L, and Deisseroth K (2019). Thirst regulates motivated behavior through modulation of brainwide neural population dynamics. Science 364, 253. [PubMed: 30948440]

Bennett C, Arroyo S, and Hestrin S (2013). Subthreshold mechanisms underlying state-dependent modulation of visual responses. Neuron 80, 350–357. [PubMed: 24139040]

Berridge KC (2004). Motivation concepts in behavioral neuroscience. Physiol. Behav. 81, 179–209. [PubMed: 15159167]

Betley JN, Xu S, Cao ZFH, Gong R, Magnus CJ, Yu Y, and Sternson SM (2015). Neurons for hunger and thirst transmit a negative-valence teaching signal. Nature 521, 180–185. [PubMed: 25915020]

Britten KH, Newsome WT, Shadlen MN, Celebrini S, and Movshon JA (1996). A relationship between behavioral choice and the visual responses of neurons in macaque MT. Vis. Neurosci. 13, 87–100. [PubMed: 8730992]

Burgess CP, Lak A, Steinmetz NA, Zatka-Haas P, Bai Reddy C, Jacobs EAK, Linden JF, Paton JJ, Ranson A, Schrö der S, et al. (2017). High-Yield Methods for Accurate Two-Alternative Visual Psychophysics in Head-Fixed Mice. Cell Rep. 20, 2513–2524. [PubMed: 28877482]

Busse L, Ayaz A, Dhruv NT, Katzner S, Saleem AB, Schölvinck ML, Zaharia AD, and Carandini M (2011). The detection of visual contrast in the behaving mouse. J. Neurosci. 31, 11351–11361. [PubMed: 21813694]

Dipoppa M, Ranson A, Krumin M, Pachitariu M, Carandini M, and Harris KD (2018). Vision and locomotion shape the interactions between neuron types in mouse visual cortex. Neuron 98, 602–615.e8. [PubMed: 29656873]

Erisken S, Vaiceliunaite A, Jurjut O, Fiorini M, Katzner S, and Busse L (2014). Effects of locomotion extend throughout the mouse early visual system. Curr. Biol. 24, 2899–2907. [PubMed: 25484299]

Guo ZV, Li N, Huber D, Ophir E, Gutnisky D, Ting JT, Feng G, and Svoboda K (2014). Flow of cortical activity underlying a tactile decision in mice. Neuron 81, 179–194. [PubMed: 24361077]

Hira R, Honkura N, Noguchi J, Maruyama Y, Augustine GJ, Kasai H, and Matsuzaki M (2009). Transcranial optogenetic stimulation for functional mapping of the motor cortex. J. Neurosci. Methods 179, 258–263. [PubMed: 19428535]

Kahneman D, and Beatty J (1966). Pupil diameter and load on memory. Science 154, 1583–1585. [PubMed: 5924930]

Leib DE, Zimmerman CA, and Knight ZA (2016). Thirst. Curr. Biol. 26, R1260–R1265. [PubMed: 27997832]

Leib DE, Zimmerman CA, Poormoghaddam A, Huey EL, Ahn JS, Lin YC, Tan CL, Chen Y, and Knight ZA (2017). The forebrain thirst circuit drives drinking through negative reinforcement. Neuron 96, 1272–1281.e4. [PubMed: 29268095]

McGinley MJ, David SV, and McCormick DA (2015a). Cortical Membrane Potential Signature of Optimal States for Sensory Signal Detection. Neuron 87, 179–192. [PubMed: 26074005]

McGinley MJ, Vinck M, Reimer J, Batista-Brito R, Zagha E, Cadwell CR, Tolias AS, Cardin JA, and McCormick DA (2015b). Waking State: Rapid Variations Modulate Neural and Behavioral Responses. Neuron 87, 1143–1161. [PubMed: 26402600]

Musall S, Kaufman MT, Juavinett AL, Gluf S, and Churchland AK (2019). Single-trial neural dynamics are dominated by richly varied movements. Nat. Neurosci. 22, 1677–1686. [PubMed: 31551604]

Niell CM, and Stryker MP (2010). Modulation of visual responses by behavioral state in mouse visual cortex. Neuron 65, 472–479. [PubMed: 20188652]

Polack PO, Friedman J, and Golshani P (2013). Cellular mechanisms of brain state-dependent gain modulation in visual cortex. Nat. Neurosci. 16, 1331–1339. [PubMed: 23872595]

Reimer J, Froudarakis E, Cadwell CR, Yatsenko D, Denfield GH, and Tolias AS (2014). Pupil fluctuations track fast switching of cortical states during quiet wakefulness. Neuron 84, 355–362. [PubMed: 25374359]

Reimer J, McGinley MJ, Liu Y, Rodenkirch C, Wang Q, McCormick DA, and Tolias AS (2016). Pupil fluctuations track rapid changes in adrenergic and cholinergic activity in cortex. Nat. Commun. 7, 13289. [PubMed: 27824036]

Salkoff DB, Zagha E, McCarthy E, and McCormick DA (2020). Movement and Performance Explain Widespread Cortical Activity in a Visual Detection Task. Cereb. Cortex 30, 421–437. [PubMed: 31711133]

Speed A, Del Rosario J, Mikail N, and Haider B (2020). Spatial attention enhances network, cellular and subthreshold responses in mouse visual cortex. Nat. Commun. 11, 505. [PubMed: 31980628]

Steinmetz NA, Zatka-Haas P, Carandini M, and Harris KD (2019). Distributed coding of choice, action and engagement across the mouse brain. Nature 576, 266–273. [PubMed: 31776518]

Vinck M, Batista-Brito R, Knoblich U, and Cardin JA (2015). Arousal and locomotion make distinct contributions to cortical activity patterns and visual encoding. Neuron 86, 740–754. [PubMed: 25892300]

Highlights

- Mice stop performing in a visual task without reaching satiation and disengage
- Contrast sensitivity and reaction times remain stable during the engaged period
- Pupil diameter does not decrease across engagement-disengagement states
- We suggest that mice perform cost-benefit analysis and can override thirst signals

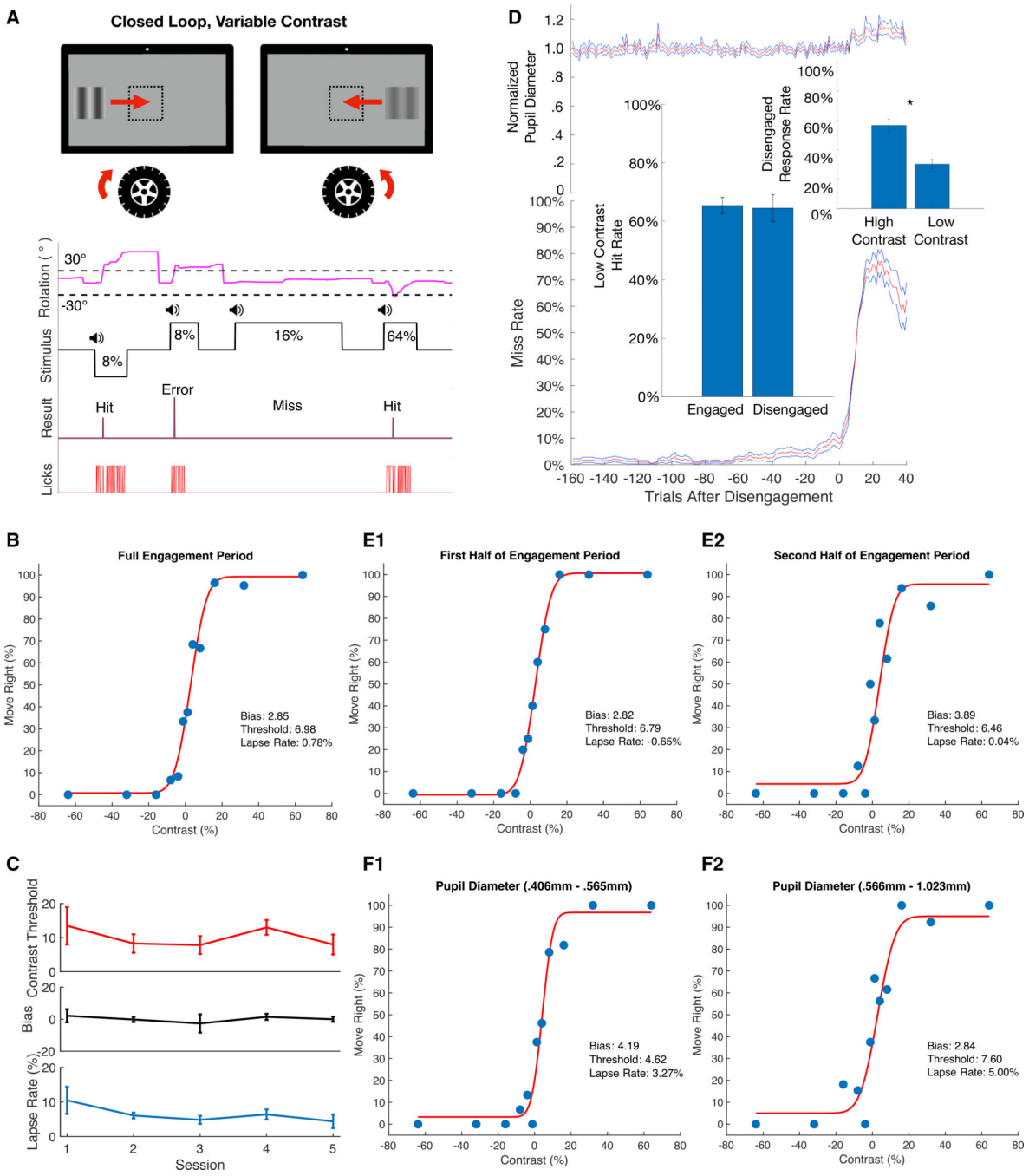

Figure 1. Mice Exhibit Sharp Transition from Engaged to Disengaged State during Behavioral Sessions

(A) Top: stationary, sinusoidal gratings of variable contrast (1.2%, 4%, 8%, 16%, 32%, and 64%) are presented on either the left or right in a square aperture, and the mouse rotates the Lego motorcycle wheel (curved red arrows) to move the gratings into the center of the screen (straight red arrows, dashed lines). Bottom: example trial structure. Top trace (magenta), wheel rotation in degrees, cued (speaker icon; positive: clockwise; negative: counterclockwise) stimulus (black trace) with % contrast (down indicates right stimulus, up indicates left stimulus), trial result (purple), and licks (red).

(B) Example of psychometric performance. Lines represent curve-fitted psychometric function (bias: 2.85; contrast threshold: 6.98; lapse rate: 0.078%). By convention, we plot contrast of left stimuli as negative.

(C) Curve-fitting parameters averaged for five mice over 5 days showing stability of mouse performance over time. Contrast threshold (mean: 10.11% ± 3.31%) (red), bias (mean: 0.16% ± 3.21%) (black), and lapse rate (mean: 6.43% ± 2.22%) (blue). Colored bars indicate ± SEM.

(D) Bottom: running miss rate (red) and ± SEM (blue) of five mice averaged over 30 sessions and aligned to the start of the disengagement period. Each point represents the miss rate averaged over 10 trials for the entirety of the session. Top: same as bottom panel but for mean pupil diameter 1 s before stimulus onset (red) and ± SEM (blue). Left inset: bar graph comparing mean pooled low-contrast (1.2%, 4%, 8%) hit rates during engagement and disengagement (0.65 ± 0.028 and 0.65 ± 0.046, respectively; $p = 0.987$), Wilcoxon sign rank test. Right inset: response rate during disengagement to high-contrast and low-contrast stimuli (0.57 and 0.30, respectively; $p = 1.18 \times 10^{-5}$)

(E1) Psychometric data for first half of an example behavioral session (bias: 2.82; contrast threshold: 6.79; lapse rate: −0.65%). (E2) Psychometric data for second half of an example behavioral session (bias: 3.99; contrast threshold: 6.48; lapse rate: 0.04%).

(F1) Psychometric data for an example session taken from trials in which mouse's mean pupil diameter during the quiescent period was less than the mean pupil diameter over the entire session, 0.406–0.565 mm (bias: 4.19; contrast threshold: 4.62; lapse rate: 3.27%). (F2) Psychometric data for example session taken from trials in which the mouse's mean pupil diameter during the quiescent period was greater than the mean pupil diameter over the entire session, 0.566–1.023 mm (bias: 2.84; contrast threshold: 7.60; lapse rate: 5.00%).

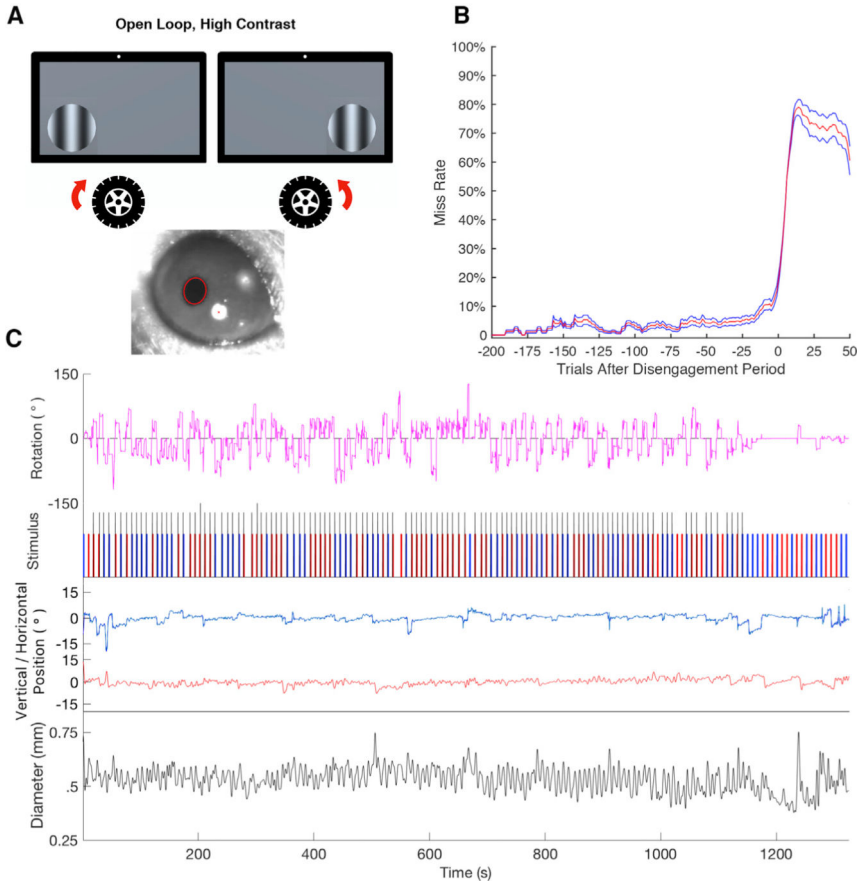

Figure 2. Open-Loop High-Contrast Task

Engaged and disengaged states show differences in variability of horizontal pupil movement, vertical pupil movement, and pupil dilation.

(A) Top: sinusoidal, drifting gratings (0.05 cycle/degree, 1.5 Hz) of fixed contrast (64%) are presented on either the left or right in circular aperture. Bottom: image of mouse's eye with pupil detection fit (red ellipse) and corneal reflection (red X).

(B) Running miss rate (red; SEM, blue) of seven mice averaged over 51 sessions.

(C) Example behavioral session showing mouse performance and pupil parameters. Wheel rotation (pink), stimulus (red: right position; blue: left position), and reward (vertical black lines). Horizontal pupil position (blue), vertical pupil position (brown), and pupil diameter (black).

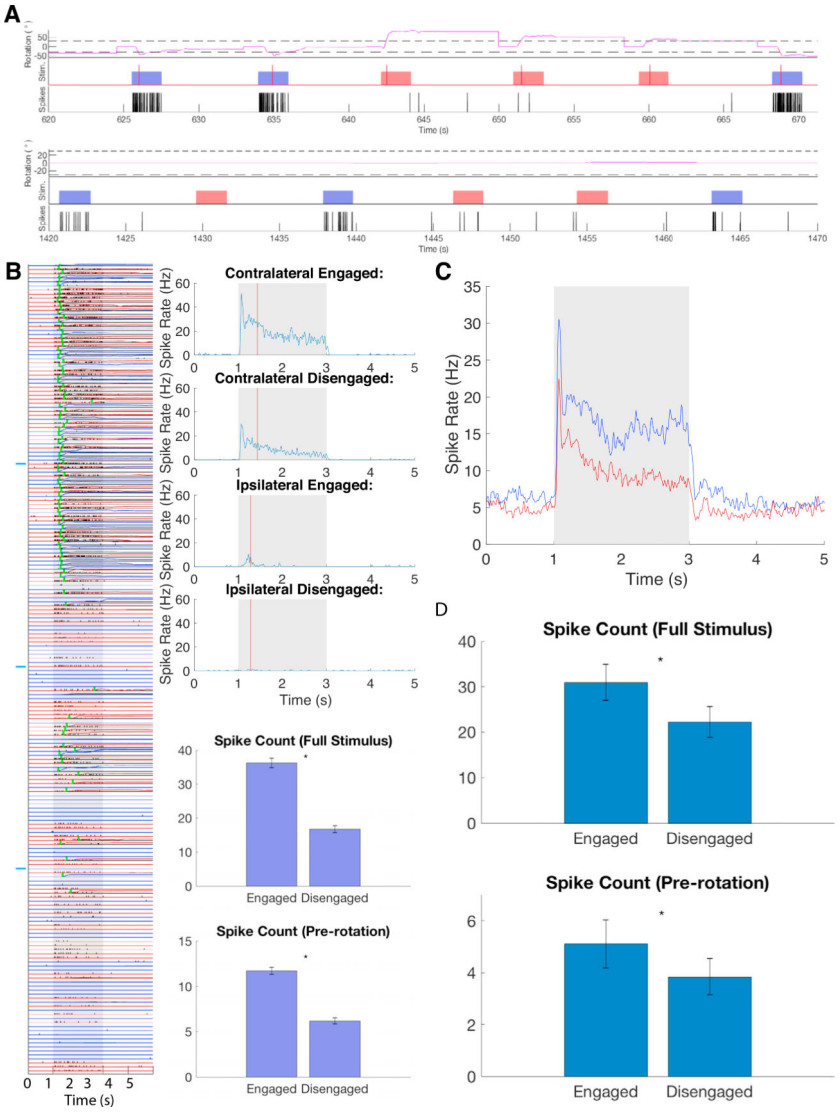

Figure 3. V1 Cells Exhibit Decreased Activity during Disengagement Period

(A) Top: example trials from engaged period. Bottom: example trials from disengaged period. Rotation (magenta), stimulus (red box: right, blue box: indicates left), reward (red vertical lines), and loose-seal detected spikes (black).

(B) Left: spike raster plot aligned to the stimulus (gray shading; open-loop; 64% contrast; preferred direction) of the cell shown in (A), for all trials in a behavioral session. Rotation (red: left rotation, blue: right rotation), rotation onset in hit trials (green), and spikes (black). Right top: Gaussian smoothed PSTH of stimulus-triggered single-unit response for engaged-period trials during contralateral stimulation, disengaged-period trials for contralateral stimulation, engaged-period trials for ipsilateral stimulation, and disengaged-period trials for ipsilateral stimulation. PSTH (blue), stimulus (grade shading), and average response latency (red vertical lines). Right bottom: comparison of spike count for full stimulus period (top) and pre-rotation period (bottom) during contralateral stimulation for engaged and disengaged trials. Spike count is significantly lower for both the full stimulus period (mean engaged: 36.21 ± 1.38; mean disengaged: 16.74 ± 1.04; $p < 10^{-7}$, Wilcoxon rank-sum test)

and pre-rotation period (mean engaged: 11.71 ± 0.37; mean disengaged: 6.19 ± 0.33; $p < 10^{-7}$, Wilcoxon rank-sum test).

(C) Grand average Gaussian-smoothed PSTH of stimulus-triggered single-unit response for engaged-period trials during contralateral stimulation (blue) and disengaged-period trials for contralateral stimulation (red). Grade shading indicates stimulus.

(D) Mean spike count for visually responsive cells is significantly larger during engagement than during disengagement (mean engaged: 30.95 ± 3.99; mean disengaged: 22.19 ± 3.39; $p = 0.033$, Wilcoxon signed rank test). Mean pre-rotation spike count is significantly larger during engagement than during disengagement (mean engaged: 5.11 ± 0.92; mean disengaged: 3.84 ± 0.70; $p = 0.009$, Wilcoxon signed rank test).

KEY RESOURCES TABLE

REAGENT or RESOURCE	SOURCE	IDENTIFIER
Experimental Models: Organisms/Strains		
C57BL/6j	JAX	N/A
VGAT-ChR2-EYFP	JAX	N/A
Software and Algorithms		
MATLAB Custom Code	Authors	N/A
Igor Pro Custom Code	Authors	N/A
Unity Custom Code	Authors	N/A
Arduino Custom Code	Authors	N/A
Other		
Custom Experimental Set-up	Authors	N/A